

North–South Asymmetry in Solar Activity and Solar Cycle Prediction, V: Prediction for the North–South Asymmetry in the Amplitude of Solar Cycle 25

J. Javaraiah¹

Abstract There exists a small but statistically significant north–south asymmetry in most of the solar activity indices and it has important implications on the solar dynamo mechanism. Here we analyzed the daily sunspot-group data reported by the Greenwich Photoheliographic Results (GPR) during the period 1874–1976, Debrecen Photoheliographic Data (DPD) during the period 1977–2017, and the revised Version-2 of international sunspot number (ISSN) during the period 1874–2017. We determined the amplitudes (the largest 13-month smoothed monthly ISSN) of Solar Cycles 12–24 and the 13-month smoothed monthly mean corrected areas of the sunspot groups in the Sun’s whole-sphere (WSGA), northern hemisphere (NSGA), and southern hemisphere (SSGA) at the epochs of the maxima of Solar Cycles 12–24. Using all these we obtained the relations similar to that found in our earlier analyzes—*i.e.* the existence of a high correlation between the sum of the areas of sunspot groups in the southern-hemisphere near-equatorial band during a small (7–9 months) interval just after a maximum epoch of a solar cycle and the amplitude of next solar cycle—separately for the Sun’s whole-sphere and northern- and southern-hemispheres. By using these relations we predict ≈ 701 msh (millionth of solar hemisphere), ≈ 429 msh, and ≈ 366 msh for the values of WSGA, NSGA, and SSGA, respectively, at the maximum epoch of Solar Cycle 25. We predict 86 ± 18 for the amplitude of Solar Cycle 25. The 13-month smoothed monthly mean sunspot-group area highly correlate with that of ISSN. Using this relation and the predicted values of WSGA, NSGA, and SSGA we obtain 68 ± 11 for the amplitude of Solar Cycle 25, which is slightly lower than the aforementioned

predicted value, and 39 ± 4 and 31 ± 6 for the values of northern- and southern-hemispheres’ sunspot numbers at the maximum epoch of Solar Cycle 25. The difference between the predicted NSGA and SSGA and also that between northern- and southern-hemispheres’ sunspot numbers at the maximum epoch of Cycle 25 are considerably small. Overall, our results suggest that the amplitude of Cycle 25 would be 25%–40% smaller, and the corresponding north–south asymmetry would be much smaller, than those of Cycle 24.

Keywords Sun: Dynamo – Sun: surface magnetism – Sun: activity – Sun: sunspots – (Sun:) space weather – (Sun:) solar–terrestrial relations

1 Introduction

Prediction of the strength of a solar cycle well in advance is important in view of the effects of solar activity on the terrestrial atmosphere and the space environment. There exists a small but statistically significant north–south asymmetry in most of the solar activity indices, such as sunspots, solar flares, prominence eruptions, coronal mass ejections, *etc.* (see Norton *et al.* 2014; Hathaway 2015). During the late Maunder minimum the north–south asymmetry was very large (Sokoloff and Nesme-Ribes 1994). Asymmetric polar field reversals may be a consequence of the asymmetry of solar activity (Svalgaard and Kamide 2013). North–south asymmetry in solar activity is also known to vary on many time scales (Vizoso and Ballester 1990; Carbonell *et al.* 1993; Verma 1993; Duchlev and Dermendjiev 1996; Javaraiah and Gokhale 1997; Knaack *et al.* 2004; Chowdhury *et al.* 2013; Ravindra and Javaraiah 2015; Chowdhury *et al.* 2016; Mandal and Banerjee 2016; Deng *et al.* 2016; Javaraiah 2019). There is also a suggestion on some systematic phase shift in the activity cycle between the hemispheres (*e.g.* Zolotova *et al.*

J. Javaraiah

¹Bikasipura, Bengaluru-560 111, India
Formerly with Indian Institute of Astrophysics, Bengaluru-560 034, India

2010; Norton and Gallagher 2010; Muraközy and Ludmány 2012; McIntosh *et al.* 2013). However, in our earlier analysis it is found that the cycle-maximum is not always occurring first in one particular hemisphere (Javaraiah 2019). The physical process responsible for the north–south asymmetry in solar activity as well as its relation to variations in solar activity is not clear yet (Volobuev and Makarenko 2017; Badalyan and Obridko 2017; Schüssler and Cameron 2018; Nepomnyashchikh *et al.* 2019). Recently, it is suggested that there could be influence of some specific configurations of the giant planets in the origin of the well-known ≈ 12 -year and 40–50-year periodicities in the north–south asymmetry of solar activity (Javaraiah 2020). North–south asymmetry in solar activity seems to have some important implications on the solar dynamo process (Sokoloff and Nesme-Ribes 1994; Belucz and Dikpati 2013; Shetye *et al.* 2015; Norton *et al.* 2014, and references therein). It seems the variations of the interplanetary magnetic field and the geomagnetic indices more closely relate with the variation of the north–south asymmetry of the solar activity than with the variation of the global activity (Muraközy 2019). Therefore, besides prediction of the amplitude of a solar cycle, prediction of the corresponding north–south asymmetry is also important for better understanding the basic processes of solar cycle and the solar–Terrestrial relationship. Attempts for predicting the north–south asymmetry based on solar dynamo models have been also made (Dikpati *et al.* 2007; Goel and Choudhuri 2009). Hathaway and Upton (2016) and Upton and Hathaway (2018) using an Advective Flux Transport code found an evidence that during Solar Cycle 25 southern hemisphere will be more active than northern hemisphere.

In our earlier analyzes (Javaraiah 2007, 2008, 2015, *i.e.* Article I, Article II, Article III) it was found that the sum of the areas of the sunspot groups in $0^\circ - 10^\circ$ latitude interval of the Sun’s southern hemisphere during the interval 1.0 to 1.75 years after the maximum epoch of a solar cycle (*i.e.* around the time of polarities change in the Sun’s global magnetic fields) correlate well with the amplitude of the next cycle. By using this relation the amplitudes of Solar Cycles 24 (Javaraiah 2007, 2008) and 25 (Javaraiah 2015, 2017) were predicted. Recently, we analyzed the combined GPR and DPD daily sunspot group data during the period 1874–2017 and determined the 13-month smoothed monthly mean corrected areas of the sunspot groups in the Sun’s whole-sphere (WSGA), northern hemisphere (NSGA), and southern hemisphere (SSGA). From these smoothed time series we had obtained the values of the maxima and minima of the WSGA-, NSGA-, and

WSGA-Cycles 12–24. We have predicted the lengths of the WSGA-Cycles (and also the lengths of corresponding sunspot cycles) 24, 25, and 26 (Javaraiah 2019, *i.e.* Article IV).

In the present article our main aim is to make a prediction for the north–south asymmetry correspond to the amplitude of the upcoming Solar Cycle 25. In all our aforementioned earlier analyzes we had used the Version-1 of ISSN. Here we have used the revised Version-2 of ISSN.

In the next section we describe the data and analysis, in Section 3 we present the results, and in Section 4 we present the conclusions and discuss them briefly.

2 Data and Analysis

We have used here the same dataset of sunspot-groups that was used in Javaraiah (2019). That is, we have analyzed the combined Greenwich and DPD sunspot-group daily data during the period April 1874–June 2017 that were downloaded from fenyi.solarobs.unideb.hu/pub/DPD/. These data contain the values of the date and the time of observation, corrected whole-spot area (A in msh: millionth of solar hemisphere), heliographic latitude (λ) and longitude (L), central meridian distance (CMD), *etc.* of sunspot groups (for details see Györi *et al.* 2010; Baranyi *et al.* 2016; Györi *et al.* 2017). In Javaraiah (2019) besides determining the actual amplitudes of WSGA-, NSGA-, and SSGA-Cycles 12–24, we have also determined the values of WSGA, NSGA, and SSGA at the epochs of the maxima (maximum values of the 13-month smoothed monthly mean ISSN, *i.e.* the values of R_M) of the Sunspot Cycles 12–24. Hereafter the values of WSGA, NSGA, and SSGA at the epoch of R_M of a sunspot cycle are denoted as A_W , A_N , and A_S , respectively. In that earlier article the values of R_M and the corresponding epoch of each of the Sunspot Cycles 12–24 were determined by using the updated time series of the 13-month smoothed monthly mean Version-1 ISSN during the period 1874–2015. It was downloaded from www.sidc.be/silso/datafiles. Here we have used the corresponding Version-2 SN time series during the period October 1874–June 2017 (used the file `SN_ms_tot_v2.0.txt`). We have also used the Version-2 SN time series of northern- and southern-hemispheres during the period July 1992–June 2017 (used the file `SN_ms_hem_V2.0.txt`). All these are also downloaded from www.sidc.be/silso/datafiles. The details of changes and corrections in Version-2 SN are given in (Clette and Lefèvre 2016). Using the Version-2 SN time series we determined the values of R_M and the

corresponding epochs of Sunspot Cycles 12–24 (which are exactly the same as the values reported in Pesnell 2018). Using these values we have determined the values of A_W , A_N , and A_S . Most of the values of R_M that are determined from the Version 2 of ISSN are different from those determined from the Version-1 of ISSN and a few of the corresponding epochs are also slightly different. Hence, at these epochs the values of A_W , A_N , and A_S are slightly different from those of the corresponding parameters of the whole sphere, northern hemisphere, and southern hemisphere, respectively, that are given in Table 1 of Javaraiah (2019). In the cases of only a few cycles the values of A_W , A_N , and A_S represent the respective maximum values of the area cycles (Javaraiah 2019).

Here we have used the same method that was used in our earlier articles for predicting the amplitudes of Solar Cycles 24 and 25 (Javaraiah 2007, 2008, 2015). We determined the correlations of the values of A_W , *i.e.* the values of WSGA at the maximum epochs of Cycles 13–24 with the sums of the areas of the sunspot groups in $0^\circ - 10^\circ$ latitude interval of the Sun’s southern hemisphere during the different time intervals that are close to the maximum epochs of Cycles 12–23. We choose the time intervals in which the sum of the area has a maximum correlation with A_W and then we obtained the linear best-fit of the area-sum and A_W . By using the obtained linear relationship and the area-sum in the time interval that is close to the maximum epoch of Cycle 24, we predicted the value of A_W of Cycle 25. Similarly, we predicted the values of A_N and A_S , *i.e.* the values of NSGA and SSGA at the maximum epoch of Solar Cycle 25. It should be noted that the values of the amplitudes and their epochs of some of the cycles are different from the corresponding values that were taken from www.ngdc.noaa.gov and were used in our earlier analyzes (Javaraiah 2007, 2008, 2015, 2017). We have already predicted the amplitude (R_M) of Cycle 25 (Javaraiah 2015, 2017). However, since we have used here a different set of the maximum values and the corresponding epochs of Solar Cycles 12–24, hence, here we have also predicted the R_M of Sunspot Cycle 25. For the sake of reducing the uncertainty in the determined sums of the areas of sunspot groups due to the foreshortening effect (if any) in the measured areas of sunspot groups, we have not used the sunspot-group data correspond to the $|CMD| > 75^\circ$. By using the predicted values of A_N and A_S of Cycle 25, we determined the corresponding north–south asymmetry, $\frac{A_N - A_S}{A_N + A_S}$. In the next section we described the results.

Here it may be worth to mention that the (linear) fits that correspond to the poorer correlations are less accurate. Hence, obviously, the predictions are less accurate and unreliable. In fact, even in the case of the

predictions based on the polar fields at minimum of cycle could more uncertain and fail if the polar fields were used early before the start of the cycle. Therefore, we have found the exact interval through partitioning the datasets until a maximum correlation is found. The sunspot-group data near the maximum of a solar cycle is well measured and the sizes of the intervals that yielded the maximum correlations are still sufficiently large (7 months and above). In addition, these intervals may have some physical significance because they comprised the epochs of polarities change in the Sun’s global magnetic fields.

For the sake of the readers convenience we listed below the meanings of all the abbreviations that are used here, because they are large.

- SN - 13-month smoothed monthly mean Version-2 ISSN during the period October 1874–June 2017,
- SN_N - 13-month smoothed monthly mean Version-2 ISSN in northern hemisphere during the period July 1992–June 2017,
- SN_S - 13-month smoothed monthly mean Version-2 ISSN in southern hemisphere during the period July 1992–June 2017,
- n - Waldmeier solar cycle number,
- T_M - maximum epoch of a solar cycle,
- R_M - value of SN at T_M ,
- σ_R - error in R_M ,
- A_W - the value of the 13-month smoothed monthly mean area of the sunspot groups in whole sphere (WSGA) at T_M ,
- A_N - the value of the 13-month smoothed monthly mean area of the sunspot groups in northern hemisphere (NSGA) at T_M ,
- A_S - the value of the 13-month smoothed monthly mean area of the sunspot groups in southern hemisphere (SSGA) at T_M ,
- T_M^* - the time-interval of 1.15 year to 1.75 year just after T_M of a cycle,
- T_W^* - the time-interval of 0.95 year to 1.6 year just after T_M of a cycle,
- T_N^* - the time-interval of 0.95 year to 1.75 year just after T_M of a cycle,
- T_S^* - the time-interval of 0.75 year to 1.65 year just after T_M of a cycle,
- A_R^* - the sum of the areas of sunspot groups in $0^\circ - 10^\circ$ latitude interval of the southern hemisphere during T_M^* of Cycle n , which has maximum correlation with R_M of Cycle $n + 1$,
- A_W^* - the sum of the areas of sunspot groups in $0^\circ - 10^\circ$ latitude interval of the southern hemisphere during T_W^* of Cycle n , which has maximum correlation with A_W of Cycle $n + 1$,

- A_N^* - the sum of the areas of sunspot groups in $0^\circ - 10^\circ$ latitude interval of the southern hemisphere during T_N^* of Cycle n , which has maximum correlation with A_N of Cycle $n + 1$,
- A_S^* - the sum of the areas of sunspot groups in $0^\circ - 10^\circ$ latitude interval of the southern hemisphere during T_S^* of Cycle n , which has maximum correlation with A_S of Cycle $n + 1$,
- T_m - the preceding minimum epoch of a cycle,
- T_m^* - the time interval around T_m of a cycle, and
- a_R^* - the sum of the areas of sunspot groups in $0^\circ - 10^\circ$ latitude interval of the northern hemisphere during T_m^* of Cycle n , which has maximum correlation with R_M of Cycle $n + 1$.

3 Results

Fig. 1 shows the cycle-to-cycle variations in A_W , A_N , A_S , and R_M . As can be seen in this figure, there exists a considerable difference between the variations in A_N and A_S . The correlation between A_N and A_S is found considerably weak (correlation coefficient $r = 0.45$). However, the correlation ($r = 0.85$) between A_N and A_W , and that ($r = 0.86$) between A_S and A_W , are found to be almost the same. In Table 1 we have given the values of A_R^* , A_W^* , A_N^* , and A_S^* , *viz.*, the sums of the areas of the sunspot groups in $0^\circ - 10^\circ$ latitude interval of the southern hemisphere during the intervals T_M^* , T_W^* , T_N^* , and T_S^* , respectively, just after T_M of a solar cycle when each of the aforementioned sums of the areas of the sunspot groups in a Cycle n well correlate with the corresponding R_M , A_W , A_N , and A_S of Cycle $n + 1$. The intervals T_M^* , T_W^* , T_N^* , and T_S^* started from the years 1.15, 0.95, 0.95, and 0.75, respectively, and ended at the years 1.75, 1.6, 1.75, and 1.65, respectively, from T_M of a cycle (T_S^* started and also ended slightly earlier than T_N^*). It should be noted that, as already mentioned above, the values of R_M , and those of T_M of some of the solar cycles, that are used here differ with those were used in the earlier analyzes (Javaraiah 2007, 2008, 2015, 2017). Therefore, the intervals T_M^* , T_W^* , T_N^* , and T_S^* of the present analysis differ with the corresponding earlier ones. However, each of these intervals of the present analysis comprised the corresponding earlier ones in large extent. The results have been specifically optimized to produce the maximum correlation. In Figure 11 of Article III, we have shown that how sensitive the results are at small variations in the exact start and stop times of the intervals over which the sums of the areas of sunspot-groups are made. There is a considerable consistency in the data sampling. That is, the intervals T_M^* , T_W^* , T_N^* , and

T_S^* are sufficiently long. Hence, small changes in the start and stop times of these intervals have no significant change in the results.

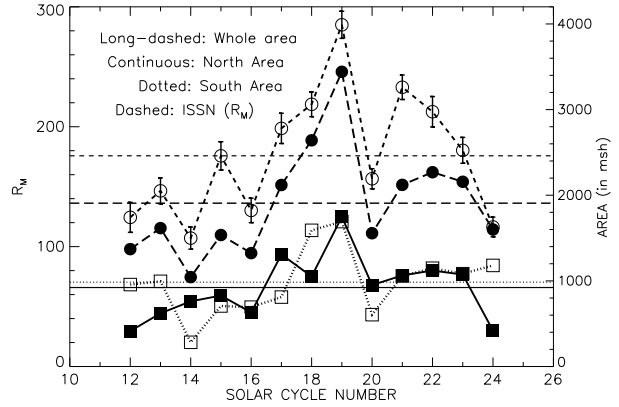


Fig. 1 Cycle-to-cycle variations in A_W (●—● curve), A_N (■—■ curve), and A_S (□··□ curve), *viz.* the 13-month smoothed monthly mean areas of the sunspot groups in the Sun's whole sphere, northern-, and southern-hemispheres, respectively, at the epoch of R_M , *i.e.* at the largest 13-month smoothed monthly mean ISSN of a solar cycle. The ○-○ curve represents the variation in R_M . The corresponding mean values of all these quantities are shown with horizontal lines. The errors in R_M are also shown. The errors in the areas of sunspot groups are not available.

In Figs. 2(a), 3(a), 4(a), and 5(a) we have compared the variations in A_R^* , A_W^* , A_N^* , and A_S^* with the variations in R_M , A_W , A_N , and A_S , respectively, during Solar Cycles 12–24. As can be seen in these figures each of the former parameters leads the corresponding one of the latter parameters by about one-cycle period. Figs. 2(b), 3(b), 4(b), and 5(b) show the correlations of A_R^* , A_W^* , A_N^* , and A_S^* of Cycle n with R_M , A_W , A_N , and A_S , respectively, of Cycle $n + 1$. The values 0.94, 0.97, 0.89 and 0.85 of the corresponding correlation coefficients are also shown. All of these correlations are significant on $>99.9\%$ confidence level ($P < 0.001$). (The corresponding Student's t values are 8.5, 12, 6, and 5.1 respectively. In the case of eleven degrees of freedom $t = 4.44$ for $P = 0.001$.) We obtained the following linear relationships.

$$R_M(n + 1) = (1.98 \pm 0.12)A_R^*(n) + 74 \pm 7, \quad (1)$$

$$A_W(n + 1) = (30.2 \pm 2.5)A_W^*(n) + 404 \pm 136, \quad (2)$$

$$A_N(n + 1) = (9.9 \pm 1.6)A_N^*(n) + 308 \pm 120, \quad (3)$$

and

$$A_S(n + 1) = (13.0 \pm 2.5)A_S^*(n) + 57 \pm 192. \quad (4)$$

Table 1 R_M represents the maximum (the largest 13-month smoothed monthly mean ISSN) and T_M is the corresponding epoch (year) of a Solar Cycle n . A_W , A_N , and A_S represent the 13-month smoothed monthly mean areas (msh) of the sunspot groups in the Sun's whole-sphere, northern hemisphere, and southern hemisphere, respectively, at T_M of a solar cycle. A_R^* , A_W^* , A_N^* , and A_S^* represent the sums of the areas (msh) of the sunspot groups (normalized by 1000) in $0^\circ - 10^\circ$ latitude intervals of the southern hemisphere during the time intervals T_M^* , T_W^* , T_N^* , and T_S^* , respectively, just after T_M of a solar cycle. σ_R represents the error in R_M . Errors in the areas of sunspot groups are not available.

n	T_M	R_M	σ_R	T_M^*	A_R^*
12	1883.958	124.4	12.5	1885.11-1885.71	30.91
13	1894.042	146.5	10.8	1895.19-1895.7	27.02
14	1906.123	107.1	9.2	1907.27-1907.87	32.34
15	1917.623	175.7	11.8	1918.77-1919.37	32.48
16	1928.290	130.2	10.2	1929.44-1930.04	70.20
17	1937.288	198.6	12.6	1938.44-1939.04	71.62
18	1947.371	218.7	10.3	1948.52-1949.12	103.85
19	1958.204	285.0	11.3	1959.35-1959.95	31.67
20	1968.874	156.6	8.4	1970.02-1970.62	72.58
21	1979.958	232.9	10.2	1981.11-1981.71	81.31
22	1989.874	212.5	12.7	1991.02-1991.62	55.36
23	2001.874	180.3	10.8	2003.02-2003.62	30.50
24	2014.288	116.4	8.2	2015.44-2016.04	6.20
		A_W		T_W^*	A_W^*
12	1883.958	1370		1884.91-1885.56	38.74
13	1894.042	1616		1894.99-1895.64	32.14
14	1906.123	1043		1907.07-1907.72	32.32
15	1917.623	1535		1918.57-1919.22	33.21
16	1928.290	1324		1929.24-1929.89	60.21
17	1937.288	2119		1938.24-1938.89	77.47
18	1947.371	2641		1948.32-1948.97	96.41
19	1958.204	3441		1959.15-1959.80	36.25
20	1968.874	1556		1969.82-1970.47	56.32
21	1979.958	2121		1980.91-1981.56	56.19
22	1989.874	2268		1990.82-1991.47	64.09
23	2001.874	2157		2002.82-2003.47	32.25
24	2014.288	1599		2015.24-2015.89	9.87
		A_N		T_N^*	A_N^*
12	1883.958	413		1884.91-1885.71	43.82
13	1894.042	621		1894.99-1895.79	34.98
14	1906.123	761		1907.07-1907.87	37.80
15	1917.623	828		1918.57-1919.37	37.14
16	1928.290	630		1929.24-1930.04	86.30
17	1937.288	1308		1938.24-1939.04	94.14
18	1947.371	1051		1948.32-1949.12	133.46
19	1958.204	1748		1959.15-1959.95	43.10
20	1968.874	951		1969.82-1970.62	76.58
21	1979.958	1063		1980.91-1981.71	97.83
22	1989.874	1120		1990.82-1991.62	69.79
23	2001.874	1073		2002.82-2003.62	43.02
24	2014.288	419		2015.24-2016.04	12.29
		A_S		T_S^*	A_S^*
12	1883.958	956		1884.71-1885.61	54.72
13	1894.042	994		1894.79-1895.69	37.45
14	1906.123	282		1906.87-1907.77	33.93
15	1917.623	706		1918.37-1919.27	41.20
16	1928.290	693		1929.04-1929.94	87.68
17	1937.288	810		1938.04-1938.94	93.25
18	1947.371	1590		1948.12-1949.02	114.50
19	1958.204	1692		1958.95-1959.85	52.97
20	1968.874	605		1969.62-1970.52	76.37
21	1979.958	1057		1980.71-1981.61	86.56
22	1989.874	1147		1990.62-1991.52	89.66
23	2001.874	1084		2002.62-2003.52	89.80
24	2014.288	1180		2015.04-2015.94	23.73

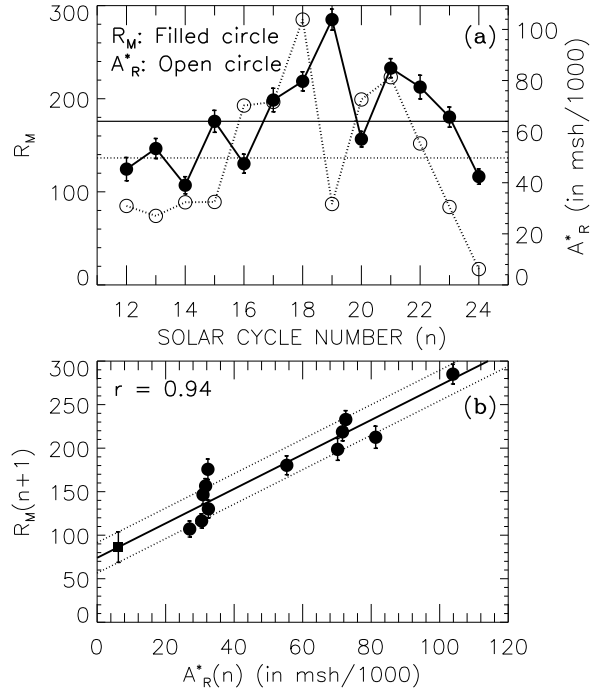


Fig. 2 (a) Plot of the amplitude (R_M), *i.e.* the largest 13-month smoothed monthly mean ISSN of a solar cycle (\bullet — \bullet curve)—and A_R^* , *i.e.* the sum of the areas of the sunspot groups in $0^\circ - 10^\circ$ latitude interval of the Sun's southern hemisphere during the interval T_M^* just after the maximum epoch T_M of a solar cycle (\circ — \circ curve)—versus the solar cycle number. (b) The scatter plot of A_R^* of a Solar Cycle n versus R_M of Solar Cycle $n+1$. The continuous line represents the corresponding linear best-fit and the dotted lines are drawn at one-rmsd (root-mean-square deviation) level. The values of the correlation coefficient (r) is also shown. The \blacksquare represents the predicted value 86 ± 18 for R_M of Cycle 25.

The fit of each of these equations to the corresponding data is reasonably good. The slopes of (1), (2), (3), and (4) are about 16, 12, 6, and 5 times larger than the corresponding uncertainties, respectively. In each of these cases, except one or two data points, all of the remaining data points are inside or close to the one-rmsd (root-mean-square deviation) level (see Figs. 2–5). Since errors (σ_R) in the values of R_M are available (see Table 1), hence, they are taken into account in the fit of 1. That is, the least-square fit is weighted with weight $= \frac{1}{\sigma_R^2}$. Errors in the areas of sunspot groups are not available. Using (1)–(4) and the values of A_R^* , A_W^* , A_N^* , and A_S^* of Cycle 24 that are given in Table 1, we obtained 86 ± 18 , 701 ± 156 msh, 429 ± 157 msh, and 366 ± 202 msh for R_M , A_W , A_N , and A_S , respectively, of Cycle 25. The rmsd values look to be substantially large for the predicted values, because the ranges of

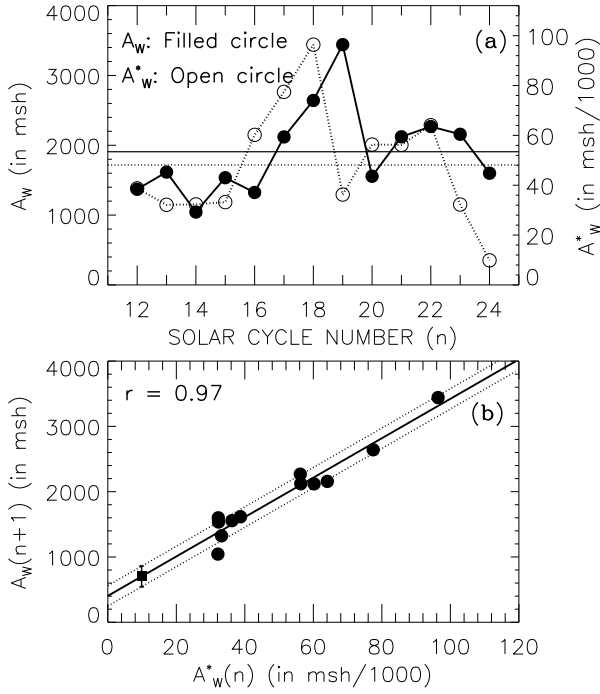


Fig. 3 (a) Plot of A_W , *i.e.* the 13-month smoothed monthly mean area of the sunspot groups in the Sun’s whole-sphere at the maximum epoch of the solar cycle ($\bullet\text{---}\bullet$ curve)– and A_W^* , *i.e.* the sum of the areas of the sunspot groups in $0^\circ - 10^\circ$ latitude interval of the southern hemisphere during the interval T_W^* just after T_M of a solar cycle ($\circ\cdots\circ$ curve)–versus the solar cycle number. (b) The scatter plot of A_W^* of a Solar Cycle n versus A_W of Solar Cycle $n + 1$. The *continuous line* represents the corresponding linear best-fit and the *dotted lines* are drawn at one-rmsd level. The values of the correlation coefficient (r) is also given. The \blacksquare represents the predicted value 701 ± 156 for A_W of Cycle 25.

A_W , A_N , and A_S values are large and the corresponding predicted values are close to the lower limits of the ranges. In Figs. 2(b), 3(b), 4(b), and 5(b) we have also shown the predicted values. These predicted values of R_M , A_W , and A_S are about $\approx 25\%$, $\approx 56\%$, and $\approx 69\%$, respectively, smaller than the corresponding observed values of Cycle 24, whereas the predicted value of A_N of Cycle 25 is almost equal to the corresponding observed value of Cycle 24. These predicted values of A_N and A_S are almost equal. Thus, the corresponding north–south asymmetry is predicted to be only 0.08. That is, there will be no significant north–south asymmetry in A_W of the upcoming Solar Cycle 25. The sum, ≈ 795 msh, of the predicted values of A_N and A_S is slightly larger than the predicted value of A_W , but the difference between this sum and the predicted value of A_W is within one-rmsd level of the latter. The predicted values, particularly, in the cases of A_N and A_S ,

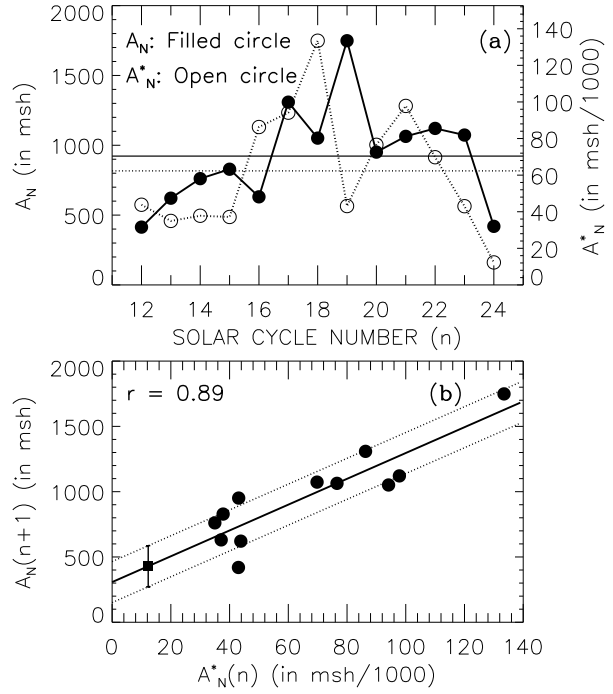


Fig. 4 (a) Plot of A_N , *i.e.* the 13-month smoothed monthly mean area of the sunspot groups in the northern hemisphere at the maximum epoch of the solar cycle ($\bullet\text{---}\bullet$ curve)– and A_N^* , *i.e.* the sum of the areas of the sunspot groups in $0^\circ - 10^\circ$ latitude interval of the southern hemisphere during the interval T_N^* just after T_M of a solar cycle ($\circ\cdots\circ$ curve)–versus the solar cycle number. (b) The scatter plot of A_N^* of a Solar Cycle n versus A_N of Solar Cycle $n + 1$. The *continuous line* represents the corresponding linear best-fit and the *dotted lines* are drawn at one-rmsd level. The values of the correlation coefficient (r) is also given. The \blacksquare represents the predicted value 429 ± 157 for A_N of Cycle 25.

have a very large uncertainties (the values of rmsd are large). However, the corresponding linear best-fits are reasonably good because the corresponding slopes are about 5–6 times larger than their respective standard deviations. The corresponding north–south asymmetry is reasonably accurate because the uncertainty in the ratio of two parameters is much smaller than the corresponding uncertainties of the individual parameters (see Javaraiah and Gokhale 1997).

The values of A_W^* , A_N^* , and A_S^* of Cycle 24 are substantially (a factor of three times) smaller than the corresponding values of all the previous cycles (see Table 1). This is consistent with that Cycle 24 is a small cycle and moreover, in the decline phase of this cycle the southern hemisphere’s activity is decreased more steeply than in the corresponding phases of other cycles (see Figure 1 in Javaraiah 2020, also see Figure 10 below). As already mentioned above, the epochs T_W^* , T_N^* , and T_S^* are close to the time of change in polar-

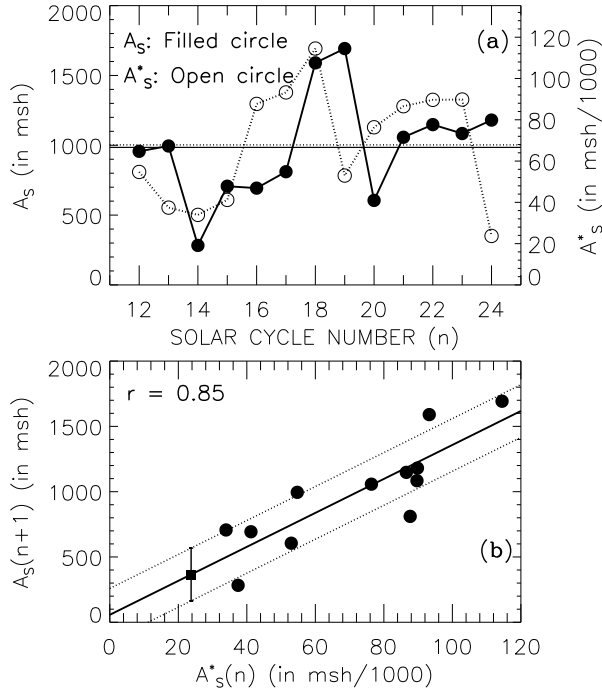


Fig. 5 (a) Plot of A_S , *i.e.* the 13-month smoothed monthly mean area of the sunspot groups in the southern hemisphere at the maximum epoch of the solar cycle (\bullet — \bullet curve)—and A_S^* , *i.e.* the sum of the areas of the sunspot groups in 0° – 10° latitude interval of the southern hemisphere during the interval T_S^* just after T_M of a solar cycle (\circ ... \circ curve)—versus the solar cycle number. (b) The scatter plot of A_S^* of a Solar Cycle n versus A_S of Solar Cycle $n+1$. The *continuous line* represents the corresponding linear best-fit and the *dotted lines* are drawn at one-rms level. The values of the correlation coefficient (r) is also given. The \blacksquare represents the predicted value 366 ± 202 for A_S of Cycle 25.

ities of global magnetic fields. In our earlier articles, (Javaraiah 2008, 2015), we have suggested equatorial crossing of magnetic flux/down flows could be a possible physical process behind all the relationships, similar to (1) above, found there. During Cycle 24 meridional motions of sunspot groups were found to be large and mostly equatorward and poleward directions in the northern- and southern-hemispheres, respectively (see Figure 1 in Javaraiah 2018). In the text of the earlier article Javaraiah (2018) the directions of the meridional motions were incorrectly mentioned as equatorward in both the hemispheres, we regret for that mistake. The meridional motions of sunspot groups may depict some extent the meridional plasma flows in the solar convection zone. Therefore, we suggest that due to the aforementioned south-bound meridional flows there might be equatorial crossing of a large northern-hemisphere magnetic flux and a large cancellation of southern-hemisphere magnetic flux. This might contributed to

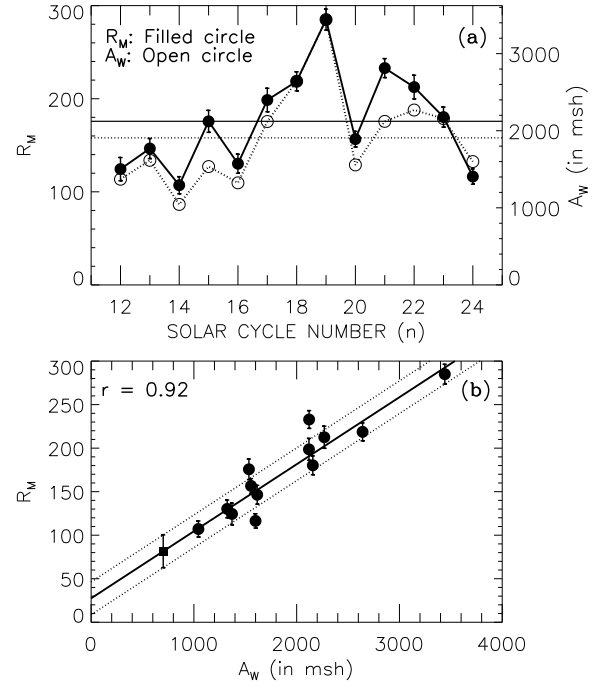


Fig. 6 (a) Plot of A_W , *i.e.* the 13-month smoothed monthly mean area of the sunspot groups in the whole-sphere at the maximum epoch of a solar cycle (\circ ... \circ curve)—and the amplitude (R_M) of the solar cycle (\bullet — \bullet curve)—versus the solar cycle number. (b) The scatter plot of A_W versus R_M . The *continuous line* represents the corresponding linear best-fit and the *dotted lines* are drawn at one-rms level. The values of the correlation coefficient (r) is also shown. The \blacksquare represents the corresponding predicted value 81 ± 19 for R_M of Cycle 25.

Cycle 24 being weaker than previous cycles and the values of A_W^* , A_N^* , and A_S^* being smaller in Cycle 24 than in previous cycles. However, sustained cross-equatorial meridional flows are ruled out by dynamical and symmetry considerations (Norton *et al.* 2014). Therefore, the physical reason behind the small values of the aforementioned parameters in Cycle 24 yet to be found.

We also determined the correlation between R_M and A_W . It is shown in Fig. 6. We found $r = 0.92$ (the corresponding Student's $t = 7.8$) and obtained the following linear relationship:

$$R_M = (0.077 \pm 0.005)A_W + 27.5 \pm 9.3. \quad (5)$$

The fit of this equation to the data is very good (in this fit error in R_M is taken into account). The slope is 15 times larger than the corresponding standard deviation. By using the value 701 msh predicted for A_W of Cycle 25 above, we have obtained 81 ± 19 for R_M of this cycle, which is almost same as the value predicted by using (1) above. Thus, overall, there is a sugges-

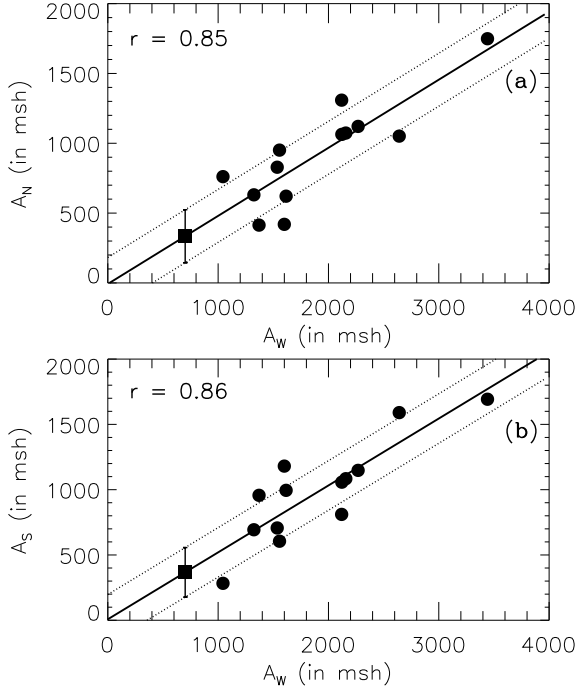


Fig. 7 The scatter plots of (a) A_W versus A_N and (b) A_W versus A_S . The *continuous line* represents the corresponding linear best-fit and the *dotted lines* are drawn at one-rmsd level. The values of the correlation coefficient (r) is also shown. The \blacksquare represents the corresponding predicted value 334 ± 190 for A_N and 467 ± 190 for A_S of Cycle 25.

tion that the amplitude of Cycle 25 will be some extent smaller than that of Cycle 24.

As already mentioned above, both A_N and A_S reasonably well correlate with A_W . By using these relationships that are shown in Fig. 7 and the value 701 msh of A_W of Cycle 25 that is predicted above, we obtained the values ≈ 334 msh and ≈ 467 msh for A_N and A_S , respectively, of Cycle 25. From these values also we get north–south asymmetry in A_W of Cycle 25 is small (-0.05), but it is a small negative value (indicates a slight more activity in south).

In our earlier analyzes, (Javaraiah 2007, 2008), we have also found that the sum (here namely a_R^*) of the areas of the sunspot groups in $0^\circ - 10^\circ$ latitude interval of the northern hemisphere—and in the time interval (namely T_m^*) -1.35 year to $+2.15$ year from the time of preceding minimum (T_m)—of Cycle n well-correlate with the R_M of Cycle $n + 1$. Although by using this relationship also we have found R_M of Cycle 24 is slightly smaller than that of Cycle 23, but it is found to be considerably higher than the observed R_M of Cycle 24. That is, this relationship in general yields a considerable over estimate for the amplitude of a cycle. From this method here we got slightly dif-

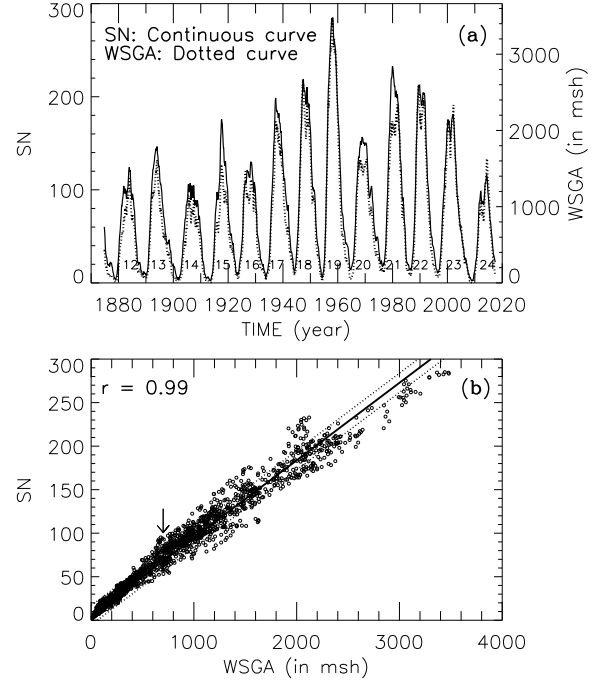


Fig. 8 (a) Plot of SN (*continuous curve*) and WSGA (*dotted curve*) *i.e.* the 13-month smoothed monthly mean values of total sunspot number (ISSN) and sunspot-group area in whole-sphere, respectively, versus the time (middle month of each 13-month interval) during the period 1875–2017. (b) The scatter plot of WSGA versus SN. The *continuous line* represents the corresponding linear best-fit and the *dotted lines* are drawn at one-rmsd level. The values of the correlation coefficient (r) is also shown. The \blacksquare (below \downarrow) at (701, 68) represents the corresponding predicted value 68 ± 11 for R_M of Cycle 25.

ferent values for T_m^* . We obtained 107 ± 25 for R_M of Cycle 25, and the values 1223 ± 233 msh, 619 ± 144 msh, and 608 ± 231 msh for A_W , A_N , and A_S of Cycle 25, respectively. The corresponding correlations are considerably smaller than those of (1)–(4), above. These values of A_N and A_S are also almost equal. That is, from this method also we obtain a negligibly small value (0.009) for the north–south asymmetry in A_W of Cycle 25. We would like to mention that the value of R_M of Cycle 24 predicted by us (Javaraiah 2007) using the method that correspond to (1) is found about 10% smaller than the observed R_M . However, in that earlier analysis we have used Solar Optical Observing Network (SOON) sunspot group data for Cycle 21–23, in which the areas of sunspot groups seem to be some extent under estimated even after increased by a factor of 1.4 (Hathaway and Choudhary 2008). There is no such problem in the DPD data. Hence, the values predicted here for the parameters of Cycle 25 by using (1)–(4) above, may be not under estimated, *i.e.* may not be

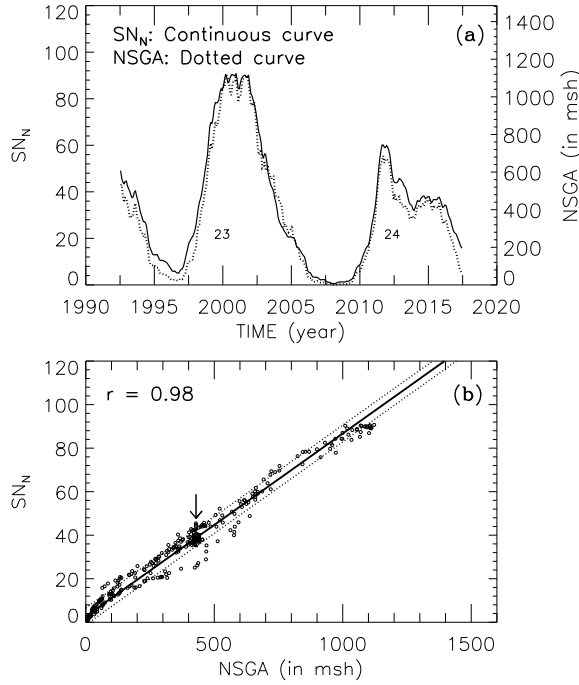


Fig. 9 (a) Plot of SN_N (*continuous curve*) and NSGA (*dotted curve*), *i.e.* the 13-month smoothed monthly mean values of ISSN and sunspot-group area, respectively, in northern-hemisphere versus time (middle month of each 13-month interval) during the period 1992–2017. (b) The scatter plot of NSGA versus SN_N . The *continuous line* represents the corresponding linear best-fit and the *dotted lines* are drawn at one-rmsd level. The values of the correlation coefficient (r) is also shown. The ■ (below ↓) at (429, 39) represents the corresponding predicted value 39 ± 4 for SN_N at the maximum epoch of Cycle 25.

about 10% smaller than the respective observed ones. Nevertheless, our predictions indicate that Cycle 25 will be at least few percent weaker than Cycle 24.

Here we would like to point out that as already mentioned above R_M of Cycle 21 is slightly larger than that of Cycle 22, whereas the behavior of A_W seems opposite to this (see Fig. 1). However, still a reasonably high correlation exists between R_M and A_W (*cf.*, Fig. 6). We have also determined the correlation between the 13-month smoothed monthly mean sunspot-group area and ISSN in whole sphere (/total), northern hemisphere, and southern hemisphere, *i.e.* the correlations between WSGA and SN, NSGA and SN_N , and SSGA and SN_S , respectively. The whole sphere has 1713 SN-values during October 1874–June 2017, whereas the northern and southern hemispheres have 300 SN_N - and SN_S -values during July 1992–June 2017. Figs. 8, 9, and 10 show the corresponding relations in the whole sphere, northern hemisphere, and southern hemisphere, respectively. In these figures the corresponding values

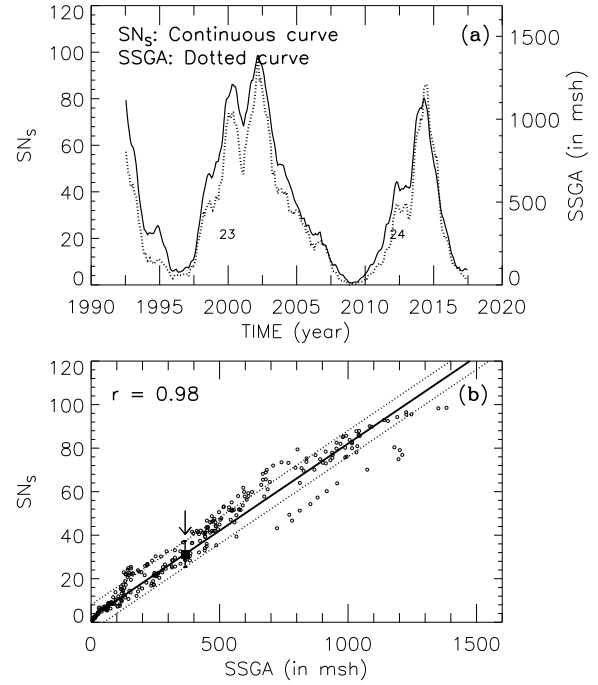


Fig. 10 (a) Plot of SN_S (*continuous curve*) and SSGA (*dotted curve*), *i.e.* the 13-month smoothed monthly mean values of ISSN and sunspot-group area, respectively, in southern-hemisphere versus time (middle month of a 13-month interval) during the period 1875–2017. (b) The scatter plot of SSGA versus SN_S . The *continuous line* represents the corresponding linear best-fit and the *dotted lines* are drawn at one-rmsd level. The values of the correlation coefficient (r) is also shown. The ■ (below ↓) at (366, 31) represents the corresponding predicted value 31 ± 6 for SN_S at the maximum epoch of Cycle 25.

0.99, 0.98, and 0.98 of r are also shown. Each of these values of r is vary high (also see Hathaway *et al.* 2002) and obviously, the corresponding linear best-fit is very good. We obtained the following relations:

$$SN = (0.089 \pm 0.0002)WSGA + 5.74 \pm 0.15, \quad (6)$$

$$SN_N = (0.084 \pm 0.0008)NSGA + 2.72 \pm 0.19, \quad (7)$$

and

$$SN_S = (0.08 \pm 0.0007)SSGA + 2.08 \pm 0.18. \quad (8)$$

In the fit of each of these equations the errors in the values of ISSN are taken into account. Using (6), (7), and (8) and the values of A_W , A_N , and A_S that are predicted from (2)–(4) above (*i.e.* the values of WSGA, NSGA, and SSAG at the epoch of R_M of Cycle 25), we obtained 68 ± 11 for R_M of Cycle 25 and 39 ± 4 and

Table 2 The values predicted for various parameters of Solar Cycle 25.

Equation	Relation between	Predicted
(1)	A_R^* (n) and R_M (n+1)	$R_M = 86 \pm 18$
(2)	A_W^* (n) and A_W (n+1)	$A_W \approx 701$
(3)	A_N^* (n) and A_N (n+1)	$A_N \approx 429$
(4)	A_S^* (n) and A_S (n+1)	$A_S \approx 366$
(5)	A_W and R_M	$R_M = 84 \pm 19$
-	A_W and A_N	$A_N \approx 334$
-	A_W and A_S	$A_S \approx 467$
(6)	WSGA and SN	$R_M = 68 \pm 11$
(7)	NSGA and SN_N	$SN_N = 39 \pm 4$
(8)	SSGA and SN_S	$SN_S = 31 \pm 6$

31 ± 6 for the values of SN_N and SN_S at the epoch of R_M of Cycle 25. It may be noted here these predicted values of SN_N and SN_S may or may not represent the values of northern- and southern-hemispheres' sunspot peaks of Cycle 25. This predicted value of R_M of Cycle 25 is some extent smaller than that predicted by using (1) above, and about 40% smaller than that of Cycle 24. This predicted value of R_M of Cycle 25 may be more accurate than that predicted from (1) because the corresponding correlation of (2) is higher than that of (1). That is, the value of A_W of Cycle 25 used in (6) is more accurately predicted from (2) than that of R_M of Cycle 25 predicted from (1). However, as can be seen in Figs. 8(a), 9(a), and 10(a) the variations in ISSN and sunspot-group area seem to be matching much better around the minimum period than around the maximum period of a cycle and it should also be noted that Waldmeier effect is not present in the cycles of sunspot-group area (Dikpati *et al.* 2008; Javaraiah 2019). The predicted value of SN_N is about 20% larger than that of SN_S . However, still there is a suggestion that the corresponding north-south asymmetry (0.11) of R_M of Solar Cycle 25 will be much smaller than the absolute value of the north-south asymmetry (-0.38) of R_M of Solar Cycle 24. Note that at the epoch of R_M of Cycle 24 the observed values of SN_N and SN_S are 36.0, and 80.4, respectively.

In Table 2 we have given the values predicted for various parameters of Solar Cycle 25. Fig. 11 shows the cycle-to-cycle variation in the corresponding north-south asymmetry of A_W , *i.e.* in $\frac{A_N - A_S}{A_N + A_S}$ and of A_W^* , *i.e.* in $\frac{A_N^* - A_S^*}{A_N^* + A_S^*}$ during Cycles 12–24. In this figure we have also shown the cycle-to-cycle variation in R_M . In addition, the predicted values of R_M and the corresponding north-south asymmetry of A_W of Cycle 25 were also shown. There exist no significant correlations be-

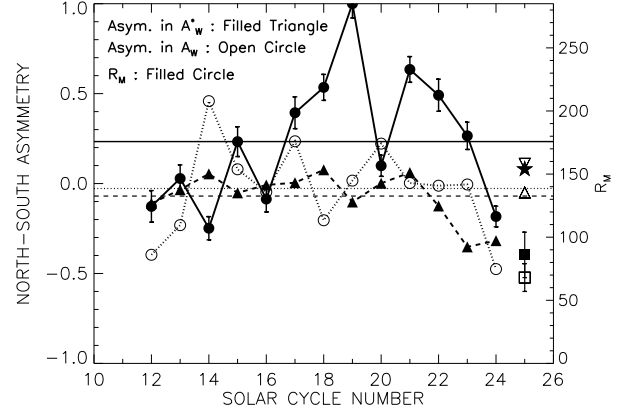


Fig. 11 Variations in the corresponding north-south asymmetry of A_W ($\circ \cdots \circ$ curve), *i.e.* in $\frac{A_N - A_S}{A_N + A_S}$ and of A_W^* ($\blacktriangle - \blacktriangle$ curve), *i.e.* in $\frac{A_N^* - A_S^*}{A_N^* + A_S^*}$ during Cycles 12–24. The $\bullet - \bullet$ curve represents the variation in R_M . The \blacksquare and \square represent the values 86 ± 18 and 68 ± 11 of R_M of Cycle 25 predicted from (1) and (6), respectively, and the ∇ represents the value 0.11 of north-south asymmetry in R_M predicted by using (7) and (8). The \star represents the value 0.08 of the corresponding north-south asymmetry in A_W of Cycle 25 predicted by using (3) and (4), and the value -0.05 that predicted by using the relations shown in Fig. 7 is represented by \triangle . A positive (negative) value of the north-south asymmetry indicates the northern (southern) hemisphere's dominance.

tween R_M and the corresponding north-south asymmetry of either A_W or A_W^* . In addition, as can be seen in Fig. 11, the corresponding asymmetry of A_W of each of Cycles 13, 17, and 20 has a considerable positive value and that of each of Cycles 12, 13, and 24 has a considerable negative value. There is a suggestion that the amplitude of Cycle 25 will have a positive or a negative very small (/negligible) north-south asymmetry similar as that correspond to the average Cycle 15 or the small Cycle 16 (see Fig. 11). Overall, there is a suggestion that there will be no significant north-south asymmetry correspond to the amplitude of Cycle 25.

Note: we have repeated all the above calculations by using Version-1 of ISSN-series and obtained the relations similar as (1)–(4), but their corresponding correlations are found better than those of (1)–(4). We found 51 ± 12 for R_M (Version-1) of Cycle 25, which is about 38% less than that (81.9) of Cycle 24 and the corresponding north-south asymmetry is also found negligible.

As mentioned in Section 1, in some cycles the northern- and southern-hemispheres typically peaks at different times, *i.e.* they are out of phase. At least one of the hemispheric maxima frequently doesn't coincide with the overall maximum. In some cycles northern-

hemisphere's peak is strong and in some other cycles southern-hemisphere's peak is strong. The strong peak is always do not occur first in the same hemisphere (Norton *et al.* 2014; Javaraiah 2019). In Figure 1 of our recent paper, Javaraiah (2020), the properties such as dominant hemisphere, phase difference between the northern- and southern-hemispheres, *etc.* of Solar Cycles 12–24 can be seen clearly. Regarding the relationships (1)–(4), we would like to point out that in the case of Cycle 24 its second SN-peak (coincided with the strong southern-hemisphere's peak) is taken into account because it is substantially larger than its first peak (coincided with the weak northern-hemisphere's peak), whereas in the case of most of the previous cycles the respective first peak is taken into account because it is larger than the corresponding second peak. Here we predicted the levels of activity in the northern- and southern-hemispheres at the epoch of the peak (R_M) of whole-sphere activity of Cycle 25. However, the hemispheres may be somewhat independent (*e.g.* Dikpati and Gilman 2001; Belucz and Dikpati 2013). Therefore, it may be necessary to make a prediction for each hemisphere's maximum independently.

4 Conclusions and Discussion

We have analyzed the daily sunspot-group data reported by GPR during the period 1874–1976, DPD during the period 1977–2017, and the revised Version-2 of ISSN during the period 1874–2017. We determined the amplitudes and corresponding epochs of Solar Cycles 12–24, and the 13-month smoothed monthly mean corrected areas of the sunspot groups in the Sun's whole-sphere (A_W), northern hemisphere (A_N), and southern hemisphere (A_S) at the epochs of the maxima of Solar Cycles 12–24. By using all these we obtained the relations—that are similar to the one found and used for predicting the amplitudes of Solar Cycles 24 and 25 in our earlier analyzes (Javaraiah 2007, 2008, 2015)—separately for the Sun's whole sphere and northern- and southern-hemispheres. Using these relations we predict the values ≈ 701 msh, ≈ 429 msh, and ≈ 366 msh for A_W , A_N , and A_S , respectively, at the maximum epochs of the upcoming Solar Cycle 25. We predict 86 ± 18 for R_M of Solar Cycle 25. The 13-month smoothed monthly mean WSGA, NSGA, and SSGA highly correlate with SN, SN_N , and SN_S , *i.e.* the corresponding total, northern-, and southern-hemispheres' sunspot numbers, respectively. Using these relations and the predicted values of A_W , A_N , and A_S we obtain 68 ± 11 for R_M of Solar Cycle 25, which is slightly lower than the aforementioned predicted value, and 39 ± 4

and 31 ± 6 for the values of SN_N and SN_S at the maximum of epoch of Solar Cycle 25. The aforementioned predicted values of R_M of Solar Cycle 25 are 20%–40% smaller than the corresponding observed values of Solar Cycle 24. The predicted values of A_W , A_S , and SN_S of Solar Cycle 25 are significantly smaller than the corresponding observed values of Solar Cycle 24, whereas the predicted values of A_N and SN_N of Solar Cycle 25 are almost equal to the corresponding observed values of Solar Cycle 24. The difference between the predicted SN_N and SN_S and also between the predicted A_N and A_S at the maximum epoch of Solar Cycle 25 are considerably small, *i.e.* the corresponding values of the north–south asymmetry are very small (0.08–0.11). In addition, A_W is found to be well correlated to both A_N and A_S . From this relationship also we get a small value (–0.05) for the corresponding north–south asymmetry in A_W of Solar Cycle 25. That is, there is a suggestion that there will be no significant north–south asymmetry in the amplitude of the upcoming Solar Cycle 25. Overall, our results suggest that the amplitude of Solar Cycle 25 would be 25%–40% smaller, and the corresponding north–south asymmetry would be much smaller, than those of Solar Cycle 24.

A number of authors have provided several explanations for the north–south asymmetry in the solar activity on both the observational and theoretical grounds (for a detail review see Norton *et al.* 2014). Recent numerical simulations from a flux transport dynamo model show the meridional circulation works differently in the northern- and southern-hemispheres in producing differing solar cycles in the northern- and southern-hemispheres (Belucz and Dikpati 2013). The flux-transport-dynamo process is the physical mechanism behind our earlier (Javaraiah 2007, 2008, 2015, 2019) and the present predictions. All our predictions are consistent with the kind of flux transport models in which a long magnetic memory is an important criteria (*e.g.* Dikpati and Gilman 2006). As suggested in our earlier articles, here also we suggest that the magnetic flux-transport by the solar meridional flows and down-flows at active regions is the main physical process behind our all predictions.

According to a kind of flux transport dynamo models the strength of the polar field at the minimum of a cycle would decide the strength of the same cycle. There exists a good correlation between the polar field at minimum epoch of cycle and the amplitude of the cycle (Jiang *et al.* 2007). Hence, the high correlation between the sum of the sunspot-group area in the southern-hemisphere near-equatorial band during the small interval just after maximum of Cycle n and the maximum of Cycle $n + 1$, implies a high correlation

between the former and the strength of the polar field at the following minimum (*i.e.* at the preceding minimum of Cycle $n + 1$). As pointed by one of the referees, the values of A_W^* , A_N^* , and A_S^* are all related to the same area on the Sun, but are so different (see Table 1) even though differences in the time intervals are very small. If the correlation actually indicates some kind of physical link, this would suggest that a very few active regions in this one narrow latitude band in the southern hemisphere over a relatively short time period are very important indicators of strength of the following cycle over many cycles. An interesting follow-up study would be to look in more detail at the cause of the differences. As already mentioned in the previous section, it might be worth thinking about cross-equatorial flux flows as well, which would be related to polar flux strength at the following minimum (Cameron *et al.* 2014).

Earlier, a cosine-fit of the amplitudes of Sunspot Cycles 1–24 indicated that Cycle 25 will take place at the minimum of the current Gleissberg cycle (Javaraiah *et al.* 2005; Javaraiah 2017). This supports a low value predicted here for the amplitude of Sunspot Cycle 25. Recently, (Javaraiah 2019), we predicted around May/2025 for the maximum epoch of Cycle 25 of sunspot-group area (Area Cycle 25). Since no significant correlation between the rise-times of sunspot- and area-cycles was found, hence, in that article we did not predict the maximum epoch of Sunspot Cycle 25. On the other hand, in Solar Cycles 22, 23, and 24—which are in the descending phase of the current Gleissberg cycle—the highest peaks of ISSN coincided with those of sunspot-group area (see Figure 8). Hence, the highest peaks of ISSN and area of Cycle 25 may coincide. Therefore, here we predict around May/2025 also for the maximum epoch of ISSN Cycle 25.

Many authors predicted the amplitude of Solar Cycle 25 by using various methods: non-linear approaches, precursors, dynamo models, *etc.* (also see Sarp *et al.* 2018; Labonville *et al.* 2019; Pishkalo 2019; Maio *et al.* 2020). In Table 3 we have given a list of some of the earlier predictions. The recent international panel of experts coordinated by the NOAA and NASA, to which the WDC-SILSO contributed, reached a consensus indicating that Cycle 25 will be most likely peak between 2023 and 2026 with a maximum sunspot number between 95 and 130. The value we have predicted here for the peak of Sunspot Cycle 25 is close to (/slightly less than) the low value indicated by the panel.

Acknowledgements The author thanks the anonymous referees of both the first and the revised versions of the manuscript for useful comments and suggestions. The author acknowledges the work of all the people

contribute and maintain the GPR and DPD Sunspot databases. The sunspot-number data are provided by WDC-SILSO, Royal Observatory of Belgium, Brussels.

Table 3 Predictions of Solar Cycle 25.

Authors	Prediction	Approach
Larger than Cycle 24:		
Helal and Galal (2012)	1.5 times of Cycle 24	From the statistics of spotless events.
Jiang and Cao (2017)	Stronger than Cycle 24	Surface flux transport model-based method.
Jiang <i>et al.</i> (2018)	93 – 155	Solar surface Flux transport dynamo model.
Sarp <i>et al.</i> (2018)	154 ± 12	The empirical dynamical modeling method to the revised Version-2 of ISSN series starting from 1749 July to 2018 January.
Pesnell and Schatten (2018)	135 ± 25	SODA Index determined by polar magnetic fields and spectral index as precursors.
Gopalswamy <i>et al.</i> (2018)	89 (south) 59 (north)	Used a precursor method (used microwave imaging observations).
Similar to Cycle 24:		
Du (2006)	102.6 ± 22.4	Maximum-maximum cycle length as an indicator to predict the amplitude.
Cameron <i>et al.</i> (2016)	Not much higher than Cycle 24	Expecting a value of dipole moment around 2020.
Wang (2017)	Similar to Cycle 24	Based on the observed evolution of polar fields and the axial dipole component of the Sun's global magnetic field at the end of 2015.
Singh and Bhargawa (2017)	102.8 ± 24.6	A statistical test for persistence of solar activity based on the value of Hurst exponent (H).
Okoh <i>et al.</i> (2018)	122.1 ± 18.2	Using the Ap-index as a precursor.
Bhowmik and Nandy (2018)	Slightly stronger than Cycle 25	Using magnetic field evolution models for the Sun's surface and interior.
Hawkes and Berger (2018)	Similar as Cycle 24	By employing magnetic helicity as a predictor.
Pishkalo (2019)	116 ± 12	Using the maximal value of filtered Wilcox Solar Observatory polar field strength before the cycle minimum as precursor.
Maio <i>et al.</i> (2020)	121	Based on the linear regression relationship between sunspot maxima and aa-index minima.
Smaller than Cycle 24:		
Javaraiah <i>et al.</i> (2005), Javaraiah (2017)	Current Gleissberg cycle's minimum	A cosine-fit of amplitudes of Cycles 1–24, <i>etc.</i>
Javaraiah (2015)	72 ± 14 (converted to Version 2)	The same as the method used in this article.
Hathaway and Upton (2016), Upton and Hathaway (2018)	A weak Cycle 25 (95 % of Cycle 24) South more than North	Using an Advective Flux Transport code.
Labonville <i>et al.</i> (2019)	89^{+29}_{-14} North 20 % more than South 6 month onset delay in North	Data-driven solar cycle model.
Covas <i>et al.</i> (2019)	57 ± 17	Based on the feed-forward artificial neural networks.
Kitiashvili (2020)	50 ± 15 (whole) ≈ 25 (south) ≈ 23 (north)	By using the Ensemble Kalman Filter method assimilated the poloidal and toroidal magnetic field components.

References

- Badalyan, O.G., Obridko, V.N.: *Astron. Astrophys.* **603**, A109 (2017)
- Baranyi, T., Györi, L., Ludmány, A.: *Sol. Phys.* **291**, 3081 (2016)
- Belucz, B., Dikpati, M.: *Astrophys. J.* **779**, 4 (2013)
- Bhowmik, P., Nandy, D.: *Nat. Commun.* **9**, A5209 (2018)
- Cameron, R.H., Jiang, J., Schüssler, M.: *Astrophys. J. Lett.* **823**, 122 (2016)
- Cameron, R.H., Jian, J., Schüssler, M., Gizon, L.: *J. Geophys. Res.* **119**, 680 (2014)
- Carbonell, M., Oliver, R., Ballester, J.L.: *Astron. Astrophys.* **274**, 497 (1993)
- Chowdhury, P., Choudhary, D. P., Gosain, S.: *Astrophys. J.* **768**, 188 (2013)
- Chowdhury, P., Gokhale, M.H., Singh, J., Moon, Y.-J.: *Astrophys. Space Sci.* **361**, 54 (2016)
- Clette, F., Lefèvre, L.: *Sol. Phys.* **291**, 2629 (2016)
- Covas, E., Peixinho, N., Fernandes, J.: *Sol. Phys.* **294**, 24 (2019)
- Deng, L.H., Xiang, Y.Y., Qu, Z.N., An, J.M.: *Astrophys. J.* **151**, 700 (2016)
- Dikpati, M., Gilman, P.A.: *Astrophys. J.* **559**, 428 (2001)
- Dikpati, M., Gilman, P.A.: *Astrophys. J.* **649**, 498 (2006)
- Dikpati, M., Gilman, P. A., de Toma, G.: *Astrophys. J. Lett.* **673**, 99 (2008)
- Dikpati, M., Gilman, P., de Toma, G., Ghosh, S.: *Sol. Phys.* **245**, 1 (2007)
- Du, Z.L.: *Astrophys. J.* **132**, 1485 (2006)
- Duchlev, P.I., Dermendjiev, V.N.: *Sol. Phys.* **168**, 205 (1996)
- Goel, A., Choudhuri, A.: *Res. Astron. Astrophys.* **9**, 115 (2009)
- Gopalswamy, N., Mäkelä, P., Yashiro, S., Akiyama, S.: *J. of Atmos. Sol. Terr. Phys.*, **176**, 26 (2018)
- Györi, L., Baranyi, T., Ludmány, A.: in *Proc. Intern. Astron. Union 6, Sympo. S273*, 403 (2010) DOI: 10.1017/s174392131101564X
- Györi, L., Ludmány, A., Baranyi, T.: *Mon. Not. R. Astron. Soc.* **465**, 1259 (2017)
- Hathaway, D.H.: *Liv. Rev. Sol. Phys.* **12**(4), 1 (2015)
- Hathaway, D.H., Choudhary, D.P.: *Sol. Phys.* **250**, 269 (2008)
- Hathaway, D.H., Upton, L.A.: *J. Geophys. Res.* **121**, 10744 (2016)
- Hathaway, D.H., Wilson, R. M., Reichmann, E.J.: *Sol. Phys.* **211**, 357 (2002)
- Hawkes, G., Berger, M. A.: *Sol. Phys.* **293**, 109 (2018)
- Helal, H.R., Galal, A.A.: *J. Advert. Res.* **4**, 275 (2012)
- Javaraiah, J.: *Mon. Not. R. Astron. Soc.* **377**, L34 (2007)
- Javaraiah, J.: *Sol. Phys.* **252**, 419 (2008)
- Javaraiah, J.: *New Astron.* **34**, 54 (2015)
- Javaraiah, J.: *Sol. Phys.* **292**, 172 (2017)
- Javaraiah, J.: in D. Banerjee, J. Jiang, K. Kusano, and S. Solanki, eds., *Long-term datasets for the Understanding of Solar and Stellar Magnetic Cycles*, *Proc. Intern. Astron. Union Symp.* 340 (2018) DOI: 10.1017/s174392131800131X
- Javaraiah, J.: *Sol. Phys.* **294**, 64 (2019)
- Javaraiah, J.: *Sol. Phys.* **295**, 8 (2020)
- Javaraiah, J., Bertello, L., Ulrich, R.: *Sol. Phys.* **232**, 25 (2005)
- Javaraiah, J., Gokhale, M.H.: *Sol. Phys.* **170**, 389 (1997)
- Jiang J., Cao J.: *J. Atmos. Sol.-Terr. Phys.*, **176**, 34 (2017)
- Jiang, J., Chatterjee, P., Choudhuri, A.R.: *Mon. Not. R. Astron. Soc.* **381**, 1527 (2007)
- Jiang, J., Wang, J.X., Jiao, Q.R., Cao, J.B.: *Astrophys. J.* **863**, 159 (2018)
- Kitiashvili, I.N.: *Astrophys. J.* **890**, 36 (2020)
- Knaack, R., Stenflo, J.O., Berdyugina, S.V.: *Astron. Astrophys.* **418**, L17 (2004)
- Labonville, F., Charbonneau, P., Lemerle, A.: *Sol. Phys.* **294**, 82 (2019)
- Miao, J., Wang, X., Ren, T.-L., Li, Z.-T.: *Res. Astron. Astrophys.* **20**, 4 (2020)
- Mandal, S., Banerjee, D.: *Astrophys. J. Lett.* **830**, L33 (2016)
- McIntosh, S.W., Leamon, R.J., Gurman, J.B., et al.: *Astrophys. J.* **765**, 146 (2013)
- Muraközy, J.: *Sol. Phys.* **294**, 46 (2019)
- Muraközy, J., Ludmány, A.: *Mon. Not. R. Astron. Soc.* **419**, 3624 (2012)
- Nepomnyashchikh, A., Mandal, S., Banerjee, D., Kitchatinov, L.: *Astron. Astrophys.* **625**, A37 (2019)
- Norton, A.A., Gallagher, J.C.: *Sol. Phys.* **261**, 193 (2010)
- Norton, A.A., Charbonneau, P., Passos, D.: *Space Sci. Rev.* **186**, 251 (2014)
- Okoh, D.I., Seemala, G.K., Rabi, A.B., Uwamahoro, J.B., Habarulema, J.B., Aggarwal, M.: *Space Weather* **16**, 1424 (2018)
- Pesnell, W.D.: *Space Weather* **16**, 1997 (2018).
- Pesnell, W.D., Schatten, K.H.: 2018, *Sol. Phys.* **293**, 112 (2018)
- Pishkalo, M.I.: *Sol. Phys.* **294**, 137 (2019)
- Ravindra, B., Javaraiah, J.: *New Astron.* **39**, 55 (2015)
- Sarp, V., Kilcik, A., Yurchyshyn, V.B., Rozelot J.P., Ozguc, A.: *Mon. Not. R. Astron. Soc.* **481**, 2981 (2018)
- Schüssler, M., Cameron, R.H.: *Astron. Astrophys.* **618**, A89 (2018)
- Shetye, J., Tripathi, D., Dikpati, M.: *Astrophys. J.* **799**, 220 (2015)
- Singh, A.K., Bhargawa, A.: *Astrophys. Space Sci.* **362**, 199 (2017)
- Sokoloff, D., Nesme-Ribes, E.: *Astron. Astrophys.* **288**, 293 (1994)
- Svalgaard, L., Kamide, Y.: *Astrophys. J.* **763**, 23 (2013)
- Upton, L.A., Hathaway, D.H.: *Geophys. Res. Lett.* **45**, 8091 (2018)
- Verma, V.K.: *Astrophys. J.* **403**, 797 (1993)
- Volobuev, D. M., Makarenko, N.G.: *Sol. Phys.* **292**, 68 (2017)
- Vizoso, G., Ballester, J.L.: *Astron. Astrophys.* **229**, 540 (1990)
- Wang, Y.-M.: *Space Sci. Rev.* **210**, 351 (2017)
- Zolotova, N.V., Ponyavin, D.I., Arlt, R., Tuominen, I.: *Astron. Nachr.* **331**, 765 (2010)